Available online at www.sciencedirect.com
ScienceDirect
Analytical Biochemistry 364 (2007) 180–192
ANALYTICAL BIOCHEMISTRY
www.elsevier.com/locate/yabio

The development of quantum dot calibration beads and quantitative multicolor bioassays in flow cytometry and microscopy

Yang Wu [a,b], Samuel K. Campos [c], Gabriel P. Lopez [b], Michelle A. Ozbun [c], Larry A. Sklar [a], Tione Buranda [a,*]

[a] Department of Pathology and Cancer Center, University of New Mexico, Albuquerque, NM 87131, USA
[b] Department of Chemical and Nuclear Engineering, University of New Mexico, Albuquerque, NM 87131, USA
[c] Department of Molecular Genetics and Microbiology, University of New Mexico, Albuquerque, NM 87131, USA

Received 22 December 2006
Available online 13 February 2007

Abstract

The use of fluorescence calibration beads has been the hallmark of quantitative flow cytometry. It has enabled the direct comparison of interlaboratory data as well as quality control in clinical flow cytometry. In this article, we describe a simple method for producing color-generalizable calibration beads based on streptavidin functionalized quantum dots. Based on their broad absorption spectra and relatively narrow emission, which is tunable on the basis of dot size, quantum dot calibration beads can be made for any fluorophore that matches their emission color. In an earlier publication, we characterized the spectroscopic properties of commercial streptavidin functionalized dots (Invitrogen). Here we describe the molecular assembly of these dots on biotinylated beads. The law of mass action is used to readily define the site densities of the dots on the beads. The applicability of these beads is tested against the industry standard, namely commercial fluorescein calibration beads. The utility of the calibration beads is also extended to the characterization surface densities of dot-labeled epidermal growth factor ligands as well as quantitative indicators of the binding of dot-labeled virus particles to cells.

Keywords: Nanotechnology; Quantum dots; Calibration beads; Flow cytometer; Quantitation; Fluorescence; Multiplex; Bioassays; Virus particles; Microscopy; Spectroscopy; Mass action

Quantum dots (Qdots)[1] are fluorescent semiconductor nanoparticles with tunable optical properties. They have very high absorption cross sections and narrow emission bandwidths, relative to fluorescent dyes, making them highly suitable for use as reporters for multiplexing assays on cells or beads [1]. There has been growing interest in the use of Qdots as fluorescent tags in biology [1,2]. One popular method for attaching dots to biological molecules involves the use of streptavidin conjugated Qdots that can be readily attached to biotinylated targets [3–7]. In general, there are 8 to 10 streptavidin molecules per quantum dot, and the size is 10 to 15 nm in diameter, which is similar

* Corresponding author. Fax: +1 505 272 6995.
E-mail address: buranda@unm.edu (T. Buranda).

[1] *Abbreviations used:* Qdot, quantum dot; RPE, retinal pigment epithelium; GFP, green fluorescent protein; MESF, molecules of equivalent soluble fluorophores; Cy5, cyanine-5; PE, phycoerythrin; EGFP, enhanced green fluorescent protein; FITC, fluorescein isothiocyanate; EGFR, epidermal growth factor receptor; HPV, human papilloma virus; PsV, pseudovirion; PFA, paraformaldehyde; PBS, phosphate-buffered saline; $FLAG^{bio}$, biotinylated FLAG; $FLAG^{FITC}$, FITC conjugated FLAG peptides; BSA, bovine serum albumin; DMEM, Dulbecco's modified Eagle's medium; FBS, fetal bovine serum; HPV16, HPV type 16; EDTA, ethylenediaminetetraacetic acid; SDS–PAGE, sodium dodecyl sulfate–polyacrylamide gel electrophoresis; TEM, transmission electron microscopy; vge, viral genome equivalents; NHS–biotin, *N*-hydroxysuccinimide ester biotin; BD, Becton Dickinson; EGF^{bio}, biotinylated EGF; HSA, human serum albumin; EGF^{fl}, fluorescein-labeled EGF; MCF, mean channel fluorescence; NIST, National Institute of Standards and Technology; EGF^{FITC}, FITC-labeled EGF ligand; DIC, differential interference contrast.

0003-2697/$ - see front matter
doi:10.1016/j.ab.2007.02.006

to the size of an antibody (~14 nm) or a large protein (e.g., retinal pigment epithelium [RPE], 240 kDa, ~20 nm) but is much larger than organic dyes (<3 nm) and small fluorescent proteins (e.g., green fluorescent protein [GFP], ~5 nm) [1].

The use of standard calibration beads to define the quantity of fluorophore-tagged ligands or proteins on cells or beads represents an essential element of quantitative flow cytometry that has enabled the direct comparison of interlaboratory data as well as quality control in clinical flow cytometry [8–11]. The utility of these standard beads is based on the correlation between the fluorescence intensity of a solution of known concentration and the intensity of a suspension of beads bearing the same fluorophores of indeterminate surface density. The equivalence of fluorescence radiance of the beads to the solution is known as the molecules of equivalent soluble fluorophores (MESF), where the MESF value is equal to the known number of molecules in solution [8,9]. To the best of our knowledge, the only commercially available sets of calibration beads are based on fluorescein, cyanine-5 (Cy5), and phycoerythrin (PE), available from Bangs Laboratories (Fiskers, IN, USA), and enhanced green fluorescent protein (EGFP), available from BD Biosciences (San Jose, CA, USA).

There is a clear need for a generalizable approach to quantifying fluorophore sites on cells or molecular assemblies on beads. In this article, we describe a simple method for producing calibration beads based on Qdots. Calibration beads can be made for any fluorophore under the operational logic that the fluorescence intensity of any given molecule is proportional to $I_0\varepsilon\phi$, where I_0 is the nonsaturating intensity of the light source. Irradiation of samples with saturating light intensities increases the potential for undesirable nonlinear effects on emission radiance as well as photobleaching of molecular probes [12–14]. ε is the absorption coefficient and ϕ is the quantum yield of the fluorophore. Calibration standards can then work on the measurement model based on the following equation (where subscripts 1 and 2 refer to the analyte and standard, respectively):

$$\frac{I_1}{I_2} = \frac{\varepsilon_{\lambda,1}}{\varepsilon_{\lambda,2}} \bullet \frac{\phi_1}{\phi_2} \bullet \frac{\%T_1}{\%T_2} \bullet \frac{\rho_1}{\rho_2}, \quad (1)$$

where I_i values are the respective intensities of the sample and standard beads excited by the same light source (I_0), ρ_i values are the site densities of the fluorophores on the Eq. (1) sample bead and the calibration bead, and $\%T$ is the percentage fraction of fluorescence light transmitted through the bandpass filter and is used to account for the spectral mismatch between the sample fluorophore and the standard. The broad absorption continuum spectra and the tunability of emission energy suggest that a dot of a suitable color can be used as a calibration reporter standard on beads for a chosen fluorophore provided that all of the spectroscopic parameters are known. This study was preceded by a systematic examination of some spectroscopic characteristics of commercially available Qdots (QD525, lot 1005-0045, and QD585, lot 0905-0031, Invitrogen, Carlsbad, CA, USA) [15]. In that study, we determined the emission yields of the quantum dot samples over a wide range of excitation wavelengths (350–500 nm). We observed an anomalous dependence of quantum yields on the excitation wavelengths, especially at wavelengths less than 420 nm. This behavior is consistent with published literature on dots [16,17]. Photoexcitation of QD585 in the wavelength window between 420 and 500 nm yielded, on average, a uniform quantum efficiency of approximately 0.20. Within the same spectral window, anomalies associated with the QD525 photoluminescence spectra were more pronounced, with the quantum yield varying from a high of approximately 0.4 at 450 nm to a low of 0.2 at 480 nm. Size heterogeneity in the dots was believed to be a significant contributor to the variation in quantum yield [15]. The data from that work are included in Table 1. We carefully noted, from our reading of the literature, that the behavior of the dots, unlike dye molecules, is susceptible to batch-to-batch variations; therefore, the data shown in Table 1 are strictly characteristic of the samples belonging to the given lot numbers.

Here we have extended our earlier work and describe a simple method for the assembly and characterization of calibration beads based on the characterized Qdots. We show that they can be used to determine the surface coverage of fluorophores, including quantum dot-tagged molecular assemblies on beads or cells by flow cytometry. Our calibration beads based on QD525 dots yielded results comparable to Bangs Laboratories' Quantum fluorescein isothiocyanate (FITC) commercial beads. For the analysis of quantum dot-labeled assemblies, we based our assays on the QD585 dots. We chose QD585 dots because of optimal spectroscopic characteristics for sensitive detection by our standard flow cytometer. We produced calibration beads of variable surface coverage spanning a range from a few hundred up to 4 million dots per bead. We tested the applicability of the calibration beads on two ligand–receptor systems of interest in the study of several forms of cancer. First, we measured the surface density of QD585 dots attached to the ligand of the epidermal growth factor receptor (EGFR) on A431 cells. EGFR has been implicated in several forms of cancer as a result of mutations involving the overexpression or constant activation of EGFR [18]. Second, we established a conceptual framework for quantitative determination of the rate of viral entry into cells by using quantum dot-labeled human papilloma virus (HPV) pseudovirion (PsV) particles. HPV has been identified as a mediator of a number of benign and malignant cancers of the skin and mucosa [19,20].

Materials and methods

Materials

Streptavidin- and biotin-coated polystyrene particles (6.7 μm in diameter, 0.5% w/v) were purchased from

Table 1
Summary of spectroscopic properties of fluorescein conjugates and QD525 (lot 1005-0045) and QD585 (lot 0905-0031) Qdots

Fluorescein	Bandwidth FWHM (nm)	λ_{ex} (nm); $\varepsilon(M^{-1}cm^{-1})$[1]	$\phi_S^2 = \phi_{ref}\frac{I_S}{I_{ref}}\frac{OD_{ref.}}{OD_S}\frac{n_S^2}{n_{ref}^2}$	% Transmittance (BP filter)[3]	Sensitivity (number of fluorescein at S/N = 3:1)[4]
$Biotin^{FITC}$	Asymmetric	488;80,000[1a]	0.82[2a]	28(530/30)[3a]	5646[4a]
$FLAG^{FITC}$			0.20[2a]		—
EGF^{FITC}			0.50[2a]		—
QD525	33	488;130,000[1b]	0.30[2a]	38(530/30)[3b]	4140[4b]
		458;216,000	0.40[2a]	48(530/30)[3c]	
		405;360,000	0.27[2b]		
		350;710,000	0.15[2b]		
QD585	28	488;530,000[1c]	0.20[2b], 0.67[2c]	65(585/42)	124[4b]
		458;1,100,000	0.20[2d]		
		405;2,200,000	0.14[2d]		
		350;3,500,000	0.10[2d]		

[1] Extinction coefficients were obtained from www.probes.invitrogen.com. (a) The extinction coefficient of fluorescein and some derivatives vary from 85,000 for the NIST fluorescein solution standard reference material SRM 1932 to 75,000 for some FITC derivatives, and values are pH dependent. We have selected a median number here. (b,c) Excitation wavelengths used in this work.

[2] Relative quantum yields (ϕ_s) were calculated using the integrated intensity of sample relative to the following. (a) Fluorescein ($\phi_{ref} = 0.95$; I_s and I_{ref} are the integrated band intensities; the optical densities of the sample and reference were similar; n is the index of refraction of the solvent [1.32 for water]). (b) ϕ_s determined from photoexcitation spectra. (c) ϕ_s determined relative to rhodamine B ($\phi_{ref} = 0.31$ in water [55]). (d) ϕ_s determined from photoexcitation spectra.

[3] Bandpass filters on a standard model BD FACScan flow cytometer. The attenuation of the fluorescein/QD525 emission by the cytometer's dichroic filter is assumed to be roughly equal. (a) Spectral mismatch between probes is negligible. (b) Emission from the excitation of QD525 at 488 nm. (c) Excitation of QD525 at 450 nm (see Ref. [15]). Filter/Probe combinations are available at www.probes.invitrogen.com.

[4] Measured using same 488 nm excitation. (a) Fluorophore site density determined from the following equation:

$$\text{Sites} = \frac{MCF_S}{MCF_{std}} \bullet \text{MESF} \bullet \frac{1}{\phi_S}, \tag{4.1}$$

using MESF values of standard Quantum MESF FITC beads. ϕ_s is the quantum yield of fluorescein biotin relative to fluorescein. The MESF values are based on the fluorescence intensity of the NIST fluorescein solution standard reference material (SRM 1932) ($\phi = 0.93$). Data supplied by Bangs Laboratories on request. (b) Derived from mass action.

Spherotech (Libertyville, IL, USA). Streptavidin-coated Qdots (QD525, QD585, and QD605) were purchased from Invitrogen. FLAG peptide (DYKDDDDK), M2 anti-FLAG antibody, and paraformaldehyde (PFA) were purchased from Sigma (St. Louis, MO, USA). Phosphate-buffered saline (PBS) was purchased from Mediatech (Herndon, VA, USA). Biotinylated FLAG ($FLAG^{bio}$) and FITC conjugated FLAG peptides ($FLAG^{FITC}$) were synthesized at the University of New Mexico as described elsewhere [21]. Tris (10 or 25 mM Tris, 150 mM NaCl, pH 7.5) and HHB (30 mM HEPES, 110 mM NaCl, 10 mM KCl, 1 mM $MgCl_26H_2O$, 10 mM glucose, pH 7.4) buffers were used in the presence or absence of 0.1% bovine serum albumin (BSA).

Cell culture

A431 cells (American Type Culture Collection, Manassas, VA, USA) and HaCaT cells (a gift from N. Fusenig, DKFZ, Heidelberg, Germany) were maintained in sterile filtered Dulbecco's modified Eagle's medium (DMEM) containing 10% heat-inactivated fetal bovine serum (FBS), 100 U/ml penicillin, 100 μg/ml streptomycin, 10 mM HEPES (pH 7.4), 20 μg/ml ciprofloxacin, and 2 mM L-glutamine at 37 °C in a CO_2 water-jacketed incubator of 5% CO_2 and 95% air (Forma Scientific, Marietta, OH, USA) in T75 tissue culture flasks or petri dishes (Greiner Bio-One, Frickenhausen, Germany). Cells typically were starved for 18 to 24 h in serum-free DMEM before experiments.

Production of biotinylated GFP-labeled HPV16 PsV particles

HPV type 16 (HPV16) PsV particles were produced as described previously [22–24]. Briefly, 293T cells were transfected with pXULL, an HPV16 L1/L2 capsid protein expression plasmid (a gift from J. Schiller, National Institutes of Health), and a "pseudogenome" reporter plasmid encoding a histone H2B–GFP fusion (a gift from H. Kimura, Tokyo Medical and Dental University) [25]. Cells were harvested 48 h posttransfection and were incubated in lysis buffer (PBS plus 9.5 mM NaCl, 0.25% Brij58, 0.3% benzonase, and 0.02 U/μl exonuclease V) for 24 h at 37 °C. PsV particles were purified by CsCl density gradient centrifugation and were dialyzed and in storage buffer (25 mM HEPES [pH 7.0], 500 mM NaCl, 0.02% Brij58, 1 mM $MgCl_2$, 0.1 mM ethylenediaminetetraacetic acid [EDTA], and 0.5% ethanol). Purity of the preparation was confirmed by sodium dodecyl sulfate–polyacrylamide gel electrophoresis (SDS–PAGE) and Coomassie staining and by negative stain transmission electron microscopy (TEM). Titer of the prep was determined by dot–blot to quantify the number of nuclease resistant pseudogenomes, as described previously [19], and is expressed in viral genome equivalents (vge). PsVs produced in this manner encapsidate the

H2B–GFP fusion protein and can be directly visualized by laser scanning confocal microscopy (S. K. Campos and M. A. Ozbun, unpublished observations).

Biotinylation of PsV

Here 8.3×10^8 vge PsV was chemically biotinylated for 1 h at room temperature by the addition of 1 μg amine reactive *N*-hydroxysuccinimide ester biotin (NHS–biotin, Pierce, Rockford, IL, USA) in 50 μl storage buffer. Excess NHS–biotin was quenched by the addition of 450 μl PBS + 50 mM glycine, and the sample was concentrated to 100 μl in storage buffer and frozen at −80 °C. The final concentration was 8.3×10^6 vge/μl.

Determination of relative emission yields of Qdots

Absorption and spectrofluorometric measurements were performed using a Hitachi model U-3270 spectrophotometer (San Jose, CA, USA) and a Photon Technology International QuantaMaster model QM-4/2005 spectrofluorometer (Lawrenceville, NJ, USA), respectively. QD525, QD585, QD605, fluorescein, FITC biotin, $FLAG^{FITC}$, and rhodamine B solutions were prepared in PBS (pH 7.4 or 8.0). The optical densities of all the samples were matched at either 405 or 488 nm. Excitation and emission spectra were collected for all samples. Fluorescence intensity data were collected at each fluorophore's emission maximum using appropriate bandpass filters (Corion, Holliston, MA, USA, and CVI Laser, Albuquerque, NM, USA).

Preparation of quantum dot-labeled microbeads

Biotinylated M2 anti-FLAG antibody-coated streptavidin beads (M2 beads) were prepared as described previously [21]. Commercially available biotinylated M2 antibodies have approximately three or four biotin conjugates on the *Fc* domain of the antibody, according to the manufacturer's data sheet. It is likely that two of the biotin groups are *cis*-bound to the streptavidin on the beads. To block extra biotins from binding to added Qdots, 20 μl of 140 nM soluble streptavidin was added to 1×10^6 M2 beads and the mixture was allowed to vortex mildly at room temperature for 15 min. The streptavidin-saturated M2 beads were then washed once in 25 mM Tris–BSA and were centrifuged at $14{,}000 \times g$ for 2 min. After removal of the supernatant, 80 μl of 1 mM biotin was added to the bead pellet and was spun down immediately after brief vortexing so as to saturate excess biotin-binding sites on the bound streptavidin. The beads were washed five times by repeated centrifugation and removal of supernatant, and they finally were resuspended in 100 μl Tris buffer before the addition of Qdots. Two interchangeable procedures were used to prepare quantum dot-labeled M2 beads using a biotinylated FLAG peptide. An aliquot of 1×10^6 M2 beads was first saturated with 100 nM $FLAG^{bio}$ at room temperature for 1 h under mild vortexing and was washed three times in Tris–BSA buffer by repeated centrifugation and removal of supernatant. After that, streptavidin-coated Qdots were added to the beads and incubated at room temperature for 1 h. The beads were then washed and resuspended in Tris buffer and were analyzed with the flow cytometer. Alternatively, a 1-μM sample of Qdots (32–40 μM streptavidin sites) was mixed with a 20-μM aliquot of $FLAG^{bio}$ and incubated in a 50-μl volume for 1 h at room temperature. The $FLAG^{bio}$/quantum dot complex was then added to M2 beads and incubated for 1 h before the beads were washed three times and analyzed. For negative control samples, the $FLAG^{bio}$ peptide was excluded from the preparation.

For samples using biotin functionalized beads, biotin-coated beads were simply mixed with the Qdots, incubated for 1 h at room temperature under mild vortexing, and washed three times in Tris–BSA. For blocked samples, biotin-coated beads were exposed to quantum dot solutions that were preblocked with soluble biotin.

Spectrofluorometric centrifugation assay

Spectrofluorometric measurements were performed in single photon counting mode. The samples were excited at either 420 or 488 nm, with a 10-nm bandpass interference filter (Corion) used for line narrowing and stray light rejection. Fluorescence emission was monitored at 520 nm via a longpass band filter (3-70 Kopp Glass, Pittsburgh, PA, USA) and a 520-nm (10-nm bandpass) filter (Corion). Neutral density filters were used to keep light intensities of the brightest samples within the dynamic range of the phototube. Samples containing 1×10^5 M2 beads or 2×10^5 biotin beads were incubated in 250 μl of 0.03, 0.1, 0.3, 1, 3, 10, 30, or 100 nM QD585 solution in Eppendorf tubes for 1 h at room temperature. The samples were then centrifuged, and the residual supernatants were collected in cylindrical glass cuvettes (Sienco, Arvada, CO, USA) for fluorescence intensity measurements. The beads were resuspended in buffer and used for flow cytometry analysis.

Eq. (2a) below was used to determine the concentration of Qdots bound to beads ($[L]_b$). I_0 and I_r are the background-corrected fluorescent intensities of Qdots before and after exposure to bead suspensions, respectively, and $[L]_0$ is the initial concentration of Qdots:

$$[L]_b = \frac{I_0 - I_r}{I_0} \bullet [L]_0 \tag{2a}$$

$$\text{Sites} = \frac{[L]_b \bullet A}{n}. \tag{2b}$$

The number of Qdots/bead was determined from Eq. (2b), where A represents Avogadro's number and n is the number of beads per liter.

Flow cytometry

Flow cytometric measurements were performed on a Becton Dickinson (BD) FACScan flow cytometer (Sunnyvale,

CA, USA) interfaced to a G4 Macintosh using the CellQuest software package. The FACScan is equipped with a 15-mW air-cooled argon ion laser. The laser output is fixed at 488 nm. In general, bead samples from the centrifugation assays were analyzed as described previously [26].

EGF and Qdot labeling of A431 cells

Cells typically were starved for 18 to 24 h in serum-free DMEM before experiments. To remove the adherent cells from the flask, cells were rinsed once and allowed to soak in sterile 0.526 mM EDTA solution (Ca^{2+} and Mg^{2+} salt free, Irvine Scientific, Santa Ana, CA, USA) at 37 °C for up to 10 min. Cells were then transferred into HHB buffer and kept in suspension for subsequent labeling and analysis. Qdot-labeled EGF ligands were formed by mixing biotinylated EGF (EGF^{bio}) with QD585 in PBS for 30 min at 7 °C under mild vortexing. Experiments were performed at several EGF^{bio}/QD585 molar ratios (1:1, 4:1, and 12:1). For binding data, QD585/EGF^{bio} complexes ranging in concentration from 1 pM to 300 nM were added to A431 cell suspensions (20,000 cells/sample), and the cells were allowed to incubate at 7 °C for 1 to 5 h under mild vortexing. Blocked samples were prepared by preincubating cells in buffers containing 0.1% BSA before exposure to QD585 (not conjugated with EGF^{bio}), and 140 μl HHB–human serum albumin (HSA) was added to cell suspensions immediately before flow cytometric analysis.

Fluorescein-labeled EGF (EGF^{fl}) ligand was purchased from Invitrogen and used without further purification. A total of 50,000 suspension A431 cells were incubated in 20 μl of 1 to 300 nM EGF^{fl} solution for 1 h at 7 °C under mild vortexing. Blocked samples were prepared by preincubation of A431 cells with at least 20 times excess of unlabeled EGF ligand (400 nM to 6 μM) at 7 °C for 1 h before exposure to EGF^{fl}, and 130 μl HHB–HSA buffer was added to the cell suspension immediately before flow cytometry analysis.

Binding of HPV16 PsV to A431 cells

Adherent cells were removed and resuspended in HHB buffer as described above. Samples containing 100,000 cells in 100 μl HHB buffer were mixed with 1×10^9 HPV16 PsV particles (10,000 PsV/cell) at 37 °C for 30 min. The cells were then washed once in HHB buffer containing 0.1% HSA before exposure to 1 nM QD585 solution in HHB. After incubation at 37 °C for 30 min, the cells were washed and analyzed.

Confocal microscopy analysis

Prestarved A431 cells were resuspended in HHB–BSA buffer ($3–5 \times 10^6$ cells/ml). For fixed cell measurements, 100 μl A431 cells was labeled with either EGF–QD585 or QD585/GFP double-tagged HPV16 PsV particles and then added to 100 μl freshly prepared cold 4% PFA in PBS. After fixing the cells in PFA for 30 min at 0 °C, the cells were washed twice in HHB–BSA buffer and spun down at 4000 rpm. The cell pellet was resuspended in 10 μl Vectashield mounting medium (Vector Laboratories, Burlingame, CA, USA) and was mounted on a regular microscope slide. Confocal laser scanning microscopy was performed with a Bio-Rad or Zeiss LSM 510 system using a 60× or 63×1.4 oil immersion objective.

Results and discussion

The fluorescence signal measured by flow cytometry usually is expressed in arbitrary mean channel fluorescence (MCF) units that are dependent on the instrument settings used in taking the measurement. Running a sample of commercially available standard calibration beads in flow cytometry experiments allows normalization of multiple data sets, even if acquired with different detector settings or on different instruments [8,9]. The utility of calibration beads lies in the application of the concept of MESF [8,9] MESF values rely on the equivalency of fluorescence intensity between a suspension of fluorophore-bearing beads and soluble fluorophores of the same species. The assignment of MESF values to a set of beads with a range of fluorophore intensities produces a calibration curve. The MESF values are based on the fluorescence properties of a native fluorophore; for example, Quantum FITC beads are based on the properties of a National Institute of Standards and Technology (NIST)-calibrated fluorescein solution. Thus, to be used accurately, the end user needs to account for the inevitable changes in quantum yields and spectral mismatches that occur when fluorescein is functionalized into a fluorescent tag [21,26].

In this study, we have developed a simple assay for producing Qdot calibration beads. The method relies on commercially available reagents, streptavidin functionalized beads, streptavidin functionalized Qdots, and the law of mass action. Because of mass action, it is possible to readily produce standard calibration beads whose site density of quantum dots spans the range from a few hundred up to 4 million dots per bead. This flexibility allows the experimenter to readily produce calibration beads with site densities of dots that are within a reasonable range of the samples under investigation. We demonstrate the utility of the beads, first, in a comparative scheme to Bangs Laboratories' Quantum FITC calibration beads and, second, in a quantitative determination of EGFR sites on A431 cells as well as in the visualization and quantification of HPV16 PsV particles tagged with Qdots on A431 cells.

Calibration and application of QD585-labeled beads

We began this work by using two types of molecular assemblies to produce calibration beads: M2 beads and biotin beads. We intended to crosscheck the utility of one platform against the other and eventually to base the application solely on biotin beads because of the reasonable

expectation that the latter beads would be generally easier to produce. The biotin beads turned out to be unsuitable because the valency of the dots (up to 8 streptavidin tetrameric units per dot) is unregulated. Because our analysis relies on mass action considerations, this problem was intractable. In addition, the flow cytometry histograms were inconsistent. The molecular assembly based on M2 beads circumvents the problem of multivalency by limiting the capture of a single dot to a single antibody in a reproducible and experimentally verifiable manner. The limiting stoichiometry is then simply reduced to the 1:1 interaction between a known quantity of antibody-binding sites on a known number of beads and a suspension of dots of known concentration (see schematic in Fig. 1A). Conceptually, the premise of a limiting 1:1 M2–Qdot binding stoichiometry is favored by the notion that the M2 antibodies and Qdots are of similar size (10–15 nm); thus, one would expect steric hindrance to limit the binding stoichiometry. This notion is supported by experimental data, as described below.

M2 beads

For several years, we have pursued methodologies concerned with the development of molecular assemblies suitable for quantitative analysis by flow cytometry. Through this effort, we developed M2 anti-FLAG-bearing beads as a platform to display and analyze, in quantitative fashion, FLAG epitope-tagged proteins on beads [21,27–31]. From our previous work, we showed that 6.7 μ streptavidin-coated beads (Spherotech) can bear approximately 4 million biotinylated antibodies at saturation when prepared under our experimental conditions [21,30]. The M2 anti-FLAG antibody binds to the FLAG (DYKDDDDK) epitope-derived peptide with an affinity constant of approximately 8 nM. In the absence of a competitor, this molecular assembly is very robust due to facile rebinding of the ligand [32–34] and remains wholly stable for days [27]. Qdots were tethered to the beads using $FLAG^{bio}$ peptides (Fig. 1A). The results of a centrifugation assay are shown in Fig. 1B, where the site density of the Qdots was derived from Eq. (2a). The maximum site coverage for QD585 was determined to be approximately 4 million dots per bead. This value matches the site density of the anti-FLAG M2 antibodies on each bead. This finding is consistent with the notion that the binding of Qdots to M2 is most likely a 1:1 binding event (Fig. 1A). The affinity constant of approximately 2 nM derived from the centrifugation assay and the parallel flow cytometric analysis of binding data on the beads (Fig. 1C) is better than that measured for monovalent interactions between M2 and soluble peptides (~8 nM) [21].

A simple law of mass action-based approach to producing calibration beads of known surface coverage

The quantitative display of streptavidin-coated Qdots on beads is regulated by the weakest affinity constant in the assembly. Thus, for a given stoichiometry of Qdots and beads, the limiting site coverage of Qdots on the M2 beads depends on the M2/FLAG affinity constant (2 nM). Conceptually, the assembly of the calibration beads is based on simple mass action considerations as shown in Eq. (3) below (where Q_0 and Q_{free} represent the initial and residual dot concentrations, respectively, and Ab and Ab_{total} represent the maximum concentration of saturable M2 sites on beads). Because a single dot occupies the bivalent M2 sites, M2 "sites" refers to the whole antibody in this case. Because the initial conditions are known $[Q]_{total}$ and K_d for the M2 beads [35] and dots, a computer simulation using Eq. (3b) can be used as a template to produce a series of beads with the desired site densities of Qdots:

$$Q + \mathrm{Ab} \underset{k_{-1}}{\overset{k_1}{\rightleftharpoons}} Q\mathrm{Ab} \tag{3a}$$

$$[Q]_0 - [Q]_{free} = [Q\mathrm{Ab}] = \frac{[\mathrm{Ab}]_{Total} \times [Q]_{free}}{[Q]_{free} + K_D} \tag{3b}$$

$$\mathrm{Sites} = \frac{[Q\mathrm{Ab}] \times A}{n} \tag{3c}$$

In practice, M2 anti-FLAG antibodies tend to lose activity over time. Therefore, one would like to keep track of the changes in the FLAG peptide–M2 interaction. We have used $FLAG^{FITC}$ [21] and commercial (Quantum FITC MESF) standard calibration beads to periodically check on the integrity of the M2 beads over time. During the course of this work, we noted a 30% drop in the activity of the M2 antibodies over a period of 6 months.

Spectroscopic characteristics of Qdots: Sensitivity and detection limits

Our effort to develop calibration beads began with a study to characterize some spectroscopic properties of streptavidin functionalized Qdots [15]. An important finding from that work was the relatively low quantum yields of the Qdots relative to fluorescein. A significant point to be made from these results was the apparent fall in quantum yields at shorter wavelengths, thereby neutralizing the potential gain in sensitivity that one would hope to get by exciting a sample in the spectral region with the highest absorption cross section. The results are summarized in Table 1. It is, however, worth noting that although the Qdots' low quantum yields negate the obvious advantage of large absorption cross section, their other advantages over organic dyes are realized in their large Stokes' shifts and relatively narrow emission bandwidths. Typical organic dyes have overlapping excitation and emission spectra with very small Stokes' shifts (e.g., 24 nm for fluorescein). To avoid spillover of excitation light, bandpass filters are designed such that they have discrete narrow bands of transmission that tend to exclude a large cross section of the emission spectrum (Fig. 2). Because Qdots have relatively much larger Stokes' shifts (up to >100 nm depending

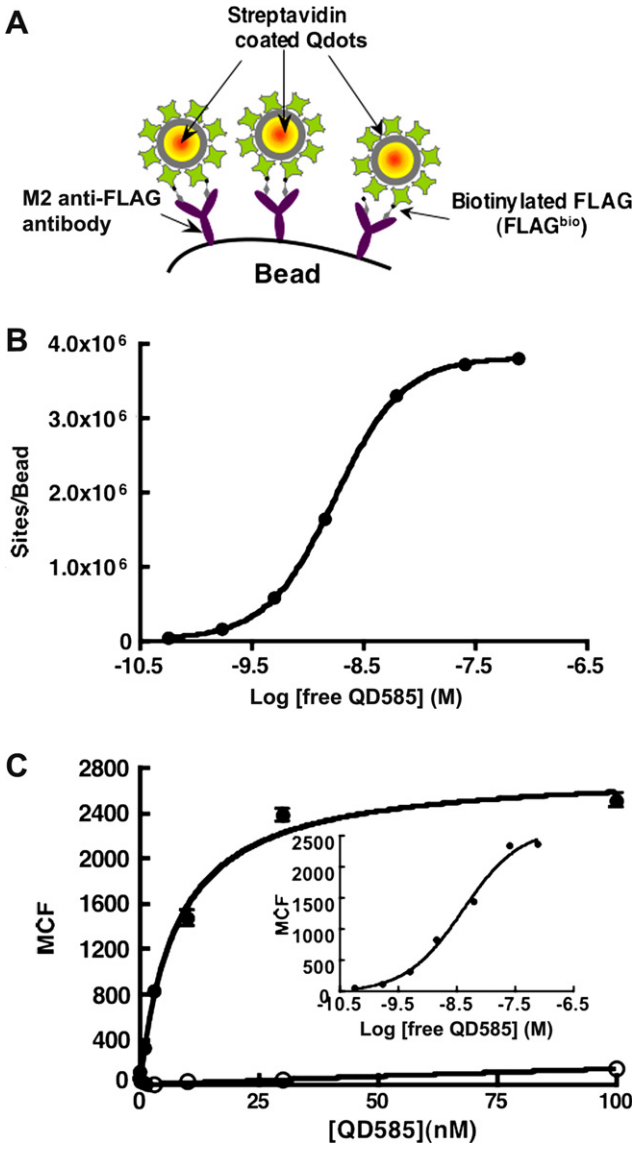

Fig. 1. (A) Limiting model schematic of a modular assembly of biotinylated M2 anti-FLAG antibodies, biotinylated FLAG peptides, and Qdots on 6.7 μm streptavidin-coated beads. Typical Qdots contain a nanoparticle core such as the CdSe, a ZnS shell for improving optical properties, and a polymer coating for isolation as well as attaching the functional group for further biological modification. The Qdot shown here is functionalized with streptavidin. The CdSe core nanocrystal typically is between 2 and 6 nm in size, depending on the emission wavelength. A typical quantum dot is conjugated to 8 to 10 streptavidin molecules, and the final size of streptavidin conjugated Qdots is between 10 and 15 nm. (B) Plot of sites/bead versus log [free QD585]. The analysis of the sigmoidal binding data from a centrifugation assay yielded a K_d of approximately 2 nM. At saturation, a site density of QD585 to approximately $4.1 \pm 0.3 \times 10^6$/bead was determined. (C) MCF signal of M2–QD585 beads versus total QD585 concentration determined by flow cytometry using beads from the previous centrifugation assay. Closed and open circles represent total binding and nonspecific binding, respectively. The sigmoidal binding curve of the cytometry data yielded a K_D value similar to that of the centrifugation assay.

on excitation wavelength) and narrow bandwidths, emission filters can be designed to capture a large percentage of their integrated emission. As shown in Fig. 2, the fluorescein spectrum has broad and asymmetric tails to the extent that 6.4% of the red edge of fluorescein's emission overlaps with FL2 bandpass. In comparison, only 0.6% of QD525 emission has the potential to bleed into FL2. Recent advances in polychromatic flow cytometry have resulted in the design and implementation of instruments capable of measuring 17 colors [36]. However, because of spectral overlap between fluorescent dyes, spillover of light between detectors inhibits the simultaneous use of all the detectors [36]. The relatively narrow band emission spectra associated with Qdots clearly are more amenable for use in multicolor flow cytometry.

Using a flow cytometer to determine the relative detection sensitivity of a prototypical fluorescein-labeled ligand, fluorescein biotin, and the dot samples QD525 and QD585, we prepared samples of beads covered with fluorophores of known surface density ranging from tens to thousands of fluorophores. The detection sensitivity (signal/noise ratio of 3:1) on our 15-year-old BD flow cytometer for fluorescein biotin was 5630 molecules/bead, for QD525 was 4100 units/bead, and for QD585 was 120 units/bead. Details of the quantification are given in the notes to Table 1. Because the experimental measure of QD525 dots/bead and fluorescein biotin molecules/bead was the product of the same 15-mW laser excitation and detection in the same spectral range (i.e., same bandpass filter), we could test the applicability of Eq. (1). We have restated Eq. (1) as Eq. (4) to reflect the identity of the two fluorophores:

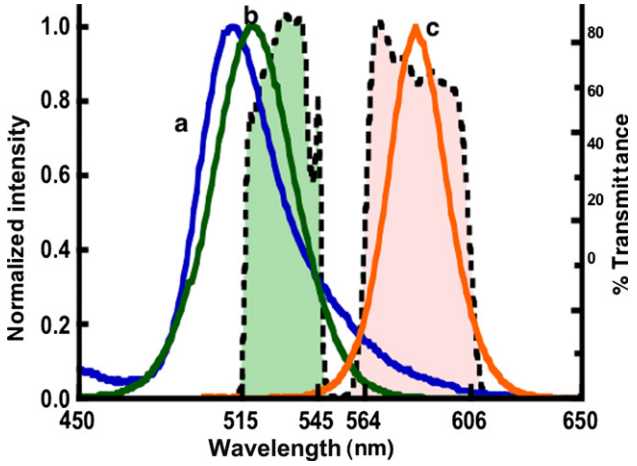

Fig. 2. Normalized emission spectra of fluorescein (curve a), QD525 (curve b), and QD585 (curve c). Green and orange bars represent bandpass filters used in a standard flow cytometer (530/30 BP for FL1, 585/42 BP for FL2). The overlap between the bandpass filters and emission spectra regulates the amount of light that is transmitted or rejected by the BP filter. Less than 30% fluorescein emission is transmitted through the FL1 filter, compared with 38% QD525 emission and 65% QD585 emission transmitted through the FL2 channel. The long tails of fluorescein emission enable the spillover of 6% of its emission into the FL2 channel. (For interpretation of the references to color in this figure legend, the reader is referred to the Web version of this article.)

$$\frac{\rho_{QD}}{\rho_{fl}} = \frac{\varepsilon_{488,QD}}{\varepsilon_{488,fl}} \bullet \frac{\phi_{QD}}{\phi_{fl}} \bullet \frac{\%T_{QD}}{\%T_{fl}} \bullet \frac{MCF_{QD}}{MCF_{fl}}. \quad (4)$$

We then calculated the ratio of the product of spectroscopic parameters (ε, ϕ, and $\%T$) of QD525 and fluorescein biotin as listed in Table 1. The MCF values were the same for the two samples. Therefore, we calculated the number of QD525 units/bead (ρ_{QD}) by taking the product of the number of fluorescein biotin molecules/bead ($\rho_{fl} = 5646$ in Table 1) and the spectroscopic parameter ratio (~0.76), and we obtained 4290. This value was within 4% of the 4140 units/bead estimated from mass action as listed in Table 1. The close agreement between independent semitheoretical expectations (Eqs. (3a)–(3c) and (4)) can be viewed as a performance validation of our Qdot calibration beads measured against the industry yardstick Quantum FITC MESF beads. It is useful to note that NIST workers have published a detailed characterization of the applicability of the MESF beads in quantitative flow cytometry [8,9] A potential source of systematic error, which we have not seriously considered here, is the error introduced by the dichroic filter as a result of spectral mismatch between the emission spectrum of the sample (fluorescein biotin) and the spectrum of the standard calibration beads or our QD525 beads. This error can be as high as 18% for a spectral shift of up to 15 nm, and it arises from changes in the transmission efficiency of the dichroic filter in a model flow cytometer in the 515- to 545-nm wavelength range delimited by the 530-nm bandpass filter [8,9] It is also instructive to note that the quantum yields of some fluorophores (e.g., fluorescein biotin) [37], octadecyl rhodamine B [38]) depend on surface density due to self-quenching at high surface occupancies [37]. Thus, unless the characteristics of surface coverage-dependent changes in fluorophore quantum yields are known, calibration beads generally are most useful at low surface densities [8,9,37].

Applicability of Qdot calibration beads on cells: Determination of EGFR sites on A431 cells using calibration QD585–M2 beads

A431 cells are human vulvar (epidermoid) carcinoma cells with high expression levels of EGFRs. We chose this cell–receptor system to test our calibration beads because there is a commercially available biotinylated EGF ligand and the receptor system has already been characterized with Qdots [39]. In addition, A431 cells are a good model system in which to study the interaction of epidermal cells with a naturally occurring multivalent ligand, namely HPVs labeled with Qdots [40,41].

In an earlier discussion in this article, we used Eq. (4) to validate the performance characteristics of our QD525 beads against those of standard MESF beads. Here we extend our characterization to cells. The issue of concern here is how the multivalent aspect of EGF ligand-bearing Qdots affects the quantitative assessment of site density and dissociation constant of the EGF ligand relative to measurements performed with a univalent FITC-labeled EGF ligand (EGF^{FITC}) characterized by MESF beads. In these experiments, we turned to QD585 dots because of their superior signal/background sensitivity relative to QD525 (Table 1).

Fig. 3 shows parabolic plots of EGF^{QD585}(1:1) and EGF^{FITC} sites per cell versus ligand concentration. It is worth noting that the signal (total bound) to background (nonspecific binding) for both data sets was greater than 10:1 (raw data not shown). The site densities were determined from our calibration beads and Quantum FITC calibration beads, respectively (cf. note 4 in Table 1). Curve b in Fig. 3 corresponds to the binding of EGF^{bio}/QD585 complexes of nominal 1:1 stoichiometry. The data indicate that the parallel incubation of equimolar amounts of EGF^{QD585}(1:1) and EGF^{FITC}, with cells producing comparable numbers of sites of bound ligand. Analysis of the parabolic data yielded the apparent binding constants (EC_{50}) of approximately 58 nM (for EGF^{FITC} [curve a in Fig. 3]) and 43 nM (for EGF^{QD585}(1:1) [curve b in Fig. 3]). The nominally lower B_{max} and K_d values associated with the EGF^{QD585} ligand may be attributable to the contribution of multivalent EGF/QD585 ligand complexes, for example, EGF^{QD585}(1:1; 2:1; 3:1; 4:1; ...). The close match between the site densities of EGF^{QD585} and EGF^{FITC} at lower ligand concentrations suggests that the univalent EGF^{QD585}(1:1) species are dominant. The site density of the receptors is compatible with the literature value of approximately 2.0×10^6 sites/cell for the A431 cell line [42]. The characteristics of multivalent interactions between EGF^{QD585} and cells are examined below.

Fig. 4A shows a parabolic plot of flow cytometry data, that is, concentration of multivalent EGF^{QD585}(12:1) versus MCF. There is an increase of two orders of magnitude in the affinity of the binding of EGF^{QD585}(12:1) to cells. We used our M2 calibration beads to derive the site number of EGF–QD585 ligand-occupied receptors from the MCF values associated with the titration. To convert the MCF

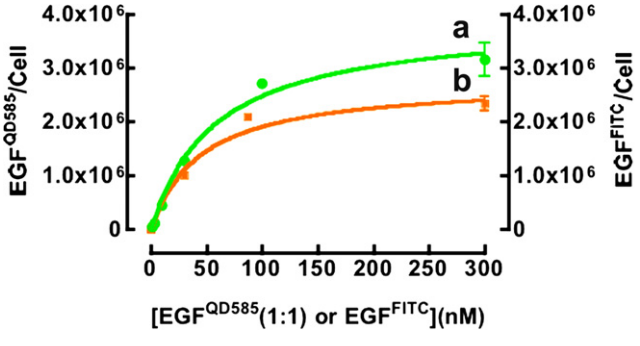

Fig. 3. Plot of EGF^{FITC} (curve a) and EGF^{QD585} (curve b) binding sites per cell versus the initial concentration of the EGF ligands. The EGF^{QD585}(1:1) ligand was formed from mixing a 1:1 molar ratio of the biotinylated EGF ligand (EGF^{bio}) and QD585 dots bearing up to 8 streptavidin units. The numbers of sites per cell were determined using standard Quantum FITC calibration beads (curve a) (cf. Table 1) and our Qdot calibration beads (curve b).

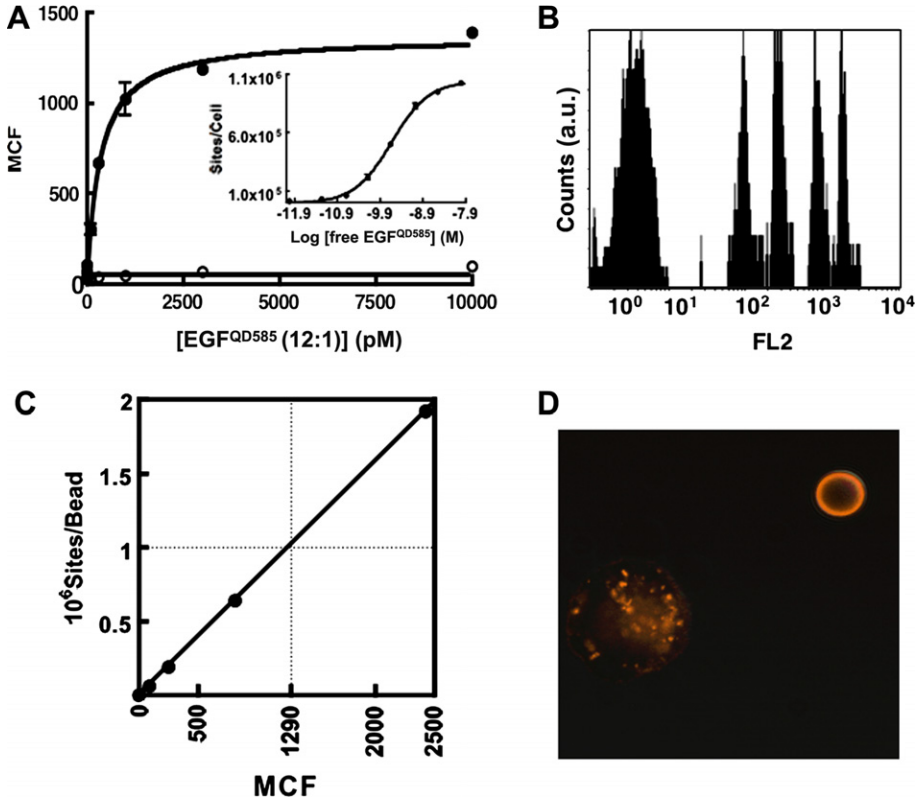

Fig. 4. Determination of total number of EGFR sites on A431 cells by flow cytometry and Qdot calibration beads. (A) Plot of MCF versus concentration of Qdot-labeled EGF ligand (EGF^{QD585}). Closed and open circles represent total binding and nonspecific binding, respectively. The inset shows a sigmoidal plot of the sites/cell versus log of free ligand. The site densities were determined from the MCF data using Qdot calibration beads. The analysis yielded a K_d of approximately 0.2 nM. (B) Flow cytometry histograms of calibration beads bearing a wide range of site densities of QD585. (C) Determination of binding sites of Qdots on A431 cells using calibration beads. A linear plot of Qdot sites on calibration beads versus the corresponding MCF reading taken at the same settings as A431 cells is shown. The intersection of the cross-hairs corresponds to the number of sites at saturation on the cells read at the y intercept. (D) Confocal microscopy image of an M2–QD585 calibration bead (top right) next to an A431 cell labeled with QD585-labeled EGF (EGF^{QD585}, middle left) for 30 min at 23 °C. The calibration bead has approximately 160,000 QD585 units, whereas the A431 cell bears approximately 100,000 Qdots.

data to site density, we produced a series of calibration beads bearing a wide range of known QD585 units. The beads were analyzed on the flow cytometer at the same detector settings for the A431 cells. The histograms are shown in Fig. 4B. A calibration curve of site densities of QD585 versus fluorescence intensities in terms of MCF was obtained through linear fitting of the MCF for the five different populations of QD585 calibration beads. The maximum site density of EGF^{QD585} was determined from the known MCF (1290) corresponding to the site density (cross-hair in Fig. 4A). The analysis gave a value of approximately 1.02×10^6 sites. Once the site occupancy was determined for the binding curve, a sigmoidal plot of the site number versus free EGF ligand was used to derive an affinity constant of 0.2 nM. It is possible that the multivalent K_d is less than 0.2 nM due to ligand depletion.

The EGF receptor has long been known to display two distinct affinities for the EGF ligand [42–48]. The high-affinity form ($K_D < 1$ nM) of the receptors comprises 1 to 10% of the receptor population. The low-affinity state has been revealed, by ^{125}I-labeled EGF studies [43–45,47,48], to span the range of K_d values between 6 and 12 nM and has been shown to be as low as 37 nM for EGF^{FITC} [42]. Our apparent K_d values for EGF^{FITC} and monovalent EGF^{QD585} (43 and 58 nM, respectively) are well within the 95% confidence interval range (30–70 nM [obtained from analysis of data in Fig. 3]) of literature measurements [42]. The normal range for K_d values found in the literature typically is the product of 6-h incubations at 4 °C. Our primary interest was not to revisit the well-characterized equilibrium binding determination of EGF but rather to determine the quantitative limits of ligand binding as measured with dots or fluorescein tags, which can be achieved by using higher than normal concentrations of ligand at shorter (2-h) incubation times. We have succeeded in this regard.

It is worth noting that the binding of EGF ligand to its cognate receptor at ambient temperature (25 °C $\leqslant$ temperature $\leqslant$ 37 °C) initiates a signaling cascade that involves the internalization of the activated receptor into endocytic vesicles of the cell [49,50]. Fig. 4D shows the confocal microscopy image of a QD585–M2 bead (160,000 Qdots/bead) next to a Qdot–EGF ligand-activated A431 cell (100,000 Qdots/cell) [51]. It would be useful to be able to

attempt a correlation of relative intensity measurements of cells and calibration beads from microscopy to flow cytometry data. However, we currently do not have the appropriate software to quantify the relative intensities of the samples accurately.

Application of QD585–M2 calibration beads: Parallel flow cytometry and fluorescence microscopy imaging of A431 cells bearing GFP- and QD585-labeled HPV16 PsV particles

HPVs are etiologic agents of a number of benign and malignant tumors of the skin and mucosa. HPV-associated human cancers include malignancies progressing from anogenital cancers, such as penile, anal, and cervical carcinomas and adenocarcinomas, and a subset of head and neck cancers. Cervical cancer is a significant cause of death and illness among women worldwide, and HPV infections are linked to more than 99% of all cervical malignancies [52]. The first act of viral infection involves the attachment of HPV and entry into cells. To elucidate the mechanisms of initial HPV entry and replication on infection and the establishment of viral persistence, one would like to establish cell-based assays for quantifying HPV infectivity. An assay based on fluorescence labeling of virus particles allows one to monitor, in real time by flow cytometry and microscopy, the early and late events of viral attachment and entry into cells. This study has begun to address some of the fundamental issues involved in establishing a quantitative Qdot-based assay to probe viral infectivity of cells.

The HPV virion consists of the chromatinized 8-kb circular double-stranded DNA genome packaged into an approximately 60-nm icosahedral capsid built from 72 L1 pentamers with 12 monomers of L2 estimated at each of the vertex positions [53,54]. Figs. 5A and B show the TEM image of purified HPV16 PsV particles and the Western blot results of biotinylated PsV detected with streptavidin–horseradish peroxidase, respectively. We recently synthesized HPV16 particles that contain histone–GFP proteins and maintain normal morphology and infectivity (see Materials and Methods). In addition to the GFP tag, this system is amenable to chemical conjugation with amine reactive probes (fluorophores or biotin). Biotinylated HPV16 PsV particles were incubated with cells for 30 min. The cells were washed and stained with QD585 and then were analyzed by flow cytometry and confocal microscopy (see Materials and Methods).

The double labeling of the virus particles with GFP and Qdots allows one to make a qualitative comparison of the two probes using a single excitation source. The data shown in Fig. 6 represent simultaneous two-color measurements of GFP/QD585 dual-stained virus particles on cells using flow cytometry and microscopy. Fig. 6A shows an overlay of flow cytometry histograms of GFP fluorescence and autofluorescence from negative control cells. As shown, the signal/background ratio is barely above 2:1. In contrast, Fig. 6B shows the measurement of QD585 units staining the same virus particle, where the fluorescence intensity of the virus particles is 10 times above that of the negative control cells. We used calibration beads to quantify the levels of GFP (~13,800 GFP/cell, standard GFP FACS calibration beads, Clontech, Palo Alto, CA, USA) and QD585 (~12,000 QD585/cell) using our M2 calibration beads. From these calibration schemes, it is worth noting that although the two probes have comparable site numbers on cells, the Qdots display a clear signal/background advantage over GFP. This advantage in sensitivity in the detection of QD585 follows the trend observed in the measurements on beads (the fourth column in Table 1).

We currently lack sufficient data to make reasonable estimates of the number of GFP molecules per particle or the extent of biotinylation; therefore, we do not know the precise number of HPV particles per cell. Currently, efforts are under way to resolve this issue with biochemical and spectroscopic methods.

Fig. 6C shows confocal images of PsV-bearing cells prepared under conditions similar to those for the flow

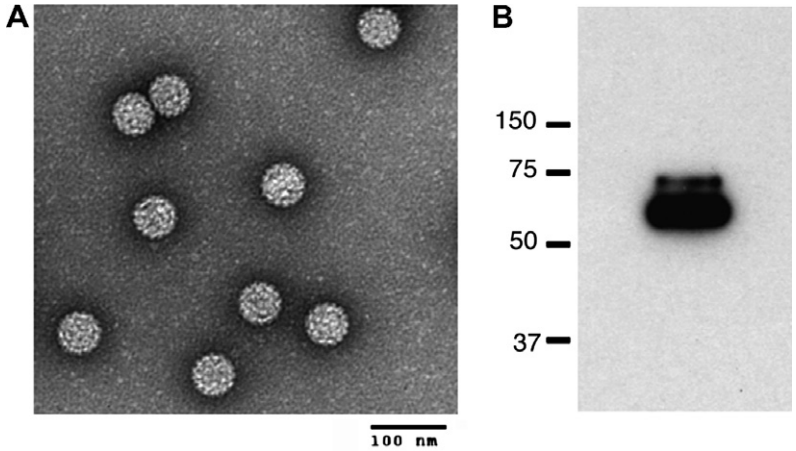

Fig. 5. (A) TEM micrograph of purified PsV preparation. Sample was negatively stained with 2% uranyl acetate. (B) Western blot of biotinylated PsV probed with streptavidin–horseradish peroxidase. Major and minor bands correspond to biotinylated L1 and L2, respectively (see text for details).

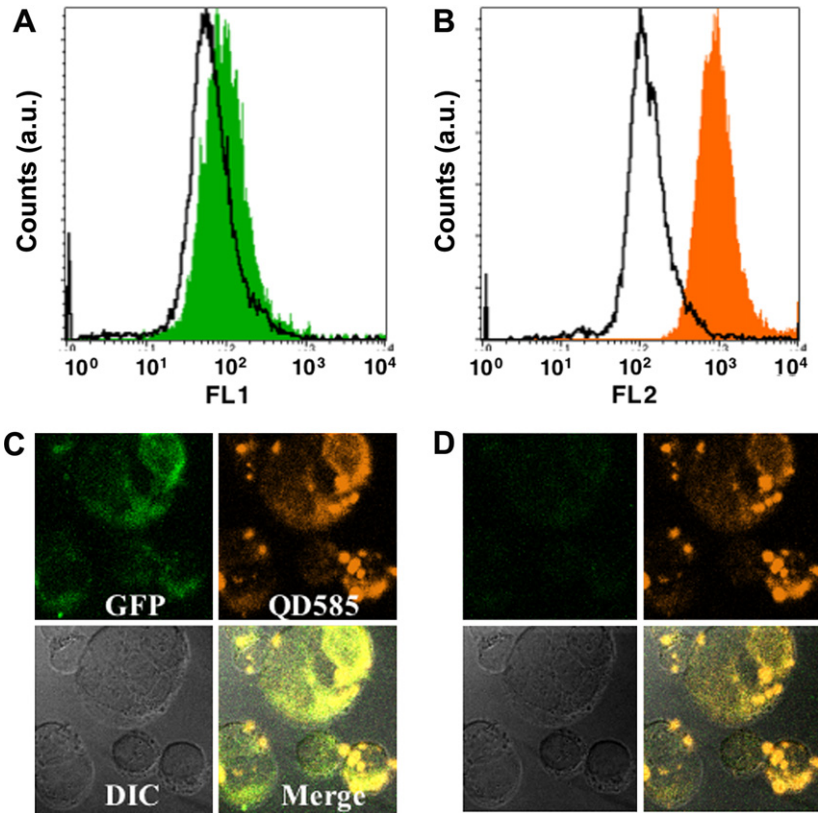

Fig. 6. Simultaneous two-color measurement of GFP/QD585 double-stained virus particles on A431 cells using flow cytometry and microscopy. (A) Flow cytometry measurement of GFP fluorescence. Solid histogram (MCF ~ 100) corresponds to cells bearing HPV particles, and open histogram (MCF ~ 50) represents negative control cells. The GFP signal is weak; at the moderate voltage setting for FL2 (600 V), crossover from GFP is minimal. (B) Fluorescence measurement of QD585. Solid histogram (MCF ~ 1100) represents cells bearing HPV particles stained with QD585, and open histogram (MCF ~ 100) represents negative control cells. Calibration beads were used to determine the level of GFP (~13,800 GFP/cell, standard GFP FACS calibration beads, Clontech) and QD585 (~12,000 QD585/cell) using our M2 calibration beads. (C) Confocal images of PsV-bearing A431 cells prepared under conditions similar to that for flow cytometry measurements. (D) Confocal images of the same cells after five scans showing the near complete photobleaching of GFP.

cytometry measurements in Figs. 6A and B. The four panels represent measures of light intensity associated with GFP (green channel) and QD585 (orange channel). Also shown are a differential interference contrast (DIC) picture and a merged image of the three panels. The colocalization of the GFP and QD585 signals is consistent with the double labeling of HPV16 PsV. Fig. 6D shows confocal images of the same cells after five scans; it displays the near complete photobleaching of GFP to background levels, whereas the orange channel signal is robust. The apparent change in intensity of the fluorescent image of QD585 is due to the diminution of detector crosstalk resulting from the ablation of GFP fluorescence.

Summary and conclusions

This work has extended the spectroscopic characterization of Qdots described in a preceding article [15] to practical development of functional calibration beads based on Qdots. The Qdot-based beads and the measurement model of Eq. (1) have a singularly important advantage over MESF beads. Because MESF beads are based on a single fluorophore entity, fluorescein (or EGFP), their utility is limited to the spectral range of fluorescein and is not applicable to the multitude of commercially available fluorophores. Because Qdots can be photoexcited at any wavelength that can be matched to a fluorophore of choice, quantitation of the target fluorophores' site coverage can be readily achieved by using Qdots whose emission spectra overlap with the target fluorophore. Because all of the Qdots are streptavidin functionalized, their production is governed by the same rules of mass action as described and demonstrated here for QD525 (using fluorescein biotin beads and Eq. 3a) and QD585 (EGFR site density characterization). Thus, multiple calibration beads can be made to order in accordance with experimental needs.

Acknowledgments

This work was supported by NIHK25AI 60036 (T.B.), NSF CTS0332315 (G.P.L.), CA85747 (M.A.O.), F32CA123842-01 (S.K.C.), and U54MH074425 (L.A.S.). We thank James Jett for critically reading an earlier version of the manuscript. Images in this article were generated in

the University of New Mexico Cancer Center Fluorescence Microscopy Facility supported by NCI P30CA118100 and as detailed on the following web site: http://kugrserver.health.unm.edu:16080/microscopy/facility.html.

References

[1] X. Michalet, F.F. Pinaud, L.A. Bentolila, J.M. Tsay, S. Doose, J.J. Li, G. Sundaresan, A.M. Wu, S.S. Gambhir, S. Weiss, Quantum dots for live cells, in vivo imaging, and diagnostics, Science 28 (2005) 538–544.
[2] X. Michalet, F. Pinaud, T.D. Lacoste, M. Dahan, M.P. Bruchez, A.P. Alivisatos, S. Weiss, Properties of fluorescent semiconductor nanocrystals and their application to biological labeling, Single Mol. 2 (2001) 261–276.
[3] W.C.W. Chan, D.J. Maxwell, X.H. Gao, R.E. Bailey, M.Y. Han, S.M. Nie, Luminescent quantum dots for multiplexed biological detection and imaging, Curr. Opin. Biotechnol. 13 (2002) 40–46.
[4] B.N.G. Giepmans, T.J. Deerinck, B.L. Smarr, Y.Z. Jones, M.H. Ellisman, Correlated light and electron microscopic imaging of multiple endogenous proteins using quantum dots, Nat. Methods 2 (2005) 743–749.
[5] I.L. Medintz, H.T. Uyeda, E.R. Goldman, H. Mattoussi, Quantum dot bioconjugates for imaging, labeling, and sensing, Nat. Mater. 4 (2005) 435–446.
[6] W.J. Parak, T. Pellegrino, C. Plank, Labelling of cells with quantum dots, Nanotechnology 16 (2005) R9–R25.
[7] D.S. Lidke, D.J. Arndt-Jovin, Imaging takes a quantum leap, Physiology 19 (2004) 322–325.
[8] A. Schwartz, A. Wang, E. Early, A.K. Gaigalas, Y. Zhang, G. Marti, R. Vogt, Quantitating fluorescence intensity from fluorophore: The definition of MESF assignment, J. Res. Natl. Inst. Stand. Technol. 107 (2002) 83–91.
[9] L. Wang, A.K. Gaigalas, F. Abbbasi, G. Marti, R. Vogt, A. Schwartz, Quantitating fluorescence intensity from fluorophores: Practical use of MESF values, J. Res. Natl. Inst. Stand. Technol. 107 (2002) 339–353.
[10] J.P. Nolan, L.A. Sklar, The emergence of flow cytometry for sensitive, real-time measurements of molecular interactions, Nat. Biotechnol. 16 (1998) 633–638.
[11] L. Sklar (Ed.), Flow Cytometry for Biotechnology, Oxford University Press, Oxford, UK, 2005.
[12] J.R. Lakowicz, Principles of Fluorescence Spectroscopy, Plenum, New York, 1999.
[13] H.M. Shapiro, Practical Flow Cytometry, Alan R. Liss, New York, 1985.
[14] C.A. Parker, Photoluminescence of Solutions, Elsevier, Amsterdam, 1968.
[15] Y. Wu, G. Lopez, L. Sklar, T. Buranda, Spectroscopic characterization of streptavidin functionalized quantum dots, Anal. Biochem. 364 (2007) 193–203.
[16] D.J. Norris, M. Nirmal, C.B. Murray, A. Sacra, M.G. Bawendi, Size-dependent optical spectroscopy of Ii–Vi semiconductor nanocrystallites (quantum dots), Zeitschrift für Physik D Atoms Molecules Clusters 26 (1993) 1–4.
[17] W. Hoheisel, V.L. Colvin, C.S. Johnson, A.P. Alivisatos, Threshold for quasi-continuum absorption and reduced luminescence efficiency in CdSe nanocrystals, J. Chem. Phys. 15 (1994) 8455–8460.
[18] J.M. Irish, R. Hovland, P. O Krutzik, O.D. Perez, O. Bruserud, B.T. Gjertsen, G.P. Nolan, Single cell profiling of potentiated phospho-protein networks in cancer cells, Cell 118 (2004) 217–228.
[19] M.A. Ozbun, Infectious human papillomavirus type 31b: Purification and infection of an immortalized human keratinocyte cell line, J. Gen. Virol. 83 (2002) 2753–2763.
[20] J.H. Lee, S.M.P. Yi, M.E. Anderson, K.L. Berger, M.J. Welsh, A.J. Klingelhutz, M.A. Ozbun, Propagation of infectious human papillomavirus type 16 by using an adenovirus and Cre/LoxP mechanism, Proc. Natl. Acad. Sci. USA 17 (2004) 2094–2099.
[21] T. Buranda, G.P. Lopez, P. Simons, A. Pastuszyn, L.A. Sklar, Detection of epitope-tagged proteins in flow cytometry: Fluorescence resonance energy transfer-based assays on beads with femtomole resolution, Anal. Biochem. 298 (2001) 151–162.
[22] C.B. Buck, D.V. Pastrana, D.R. Lowy, J.T. Schiller, Efficient intracellular assembly of papillomaviral vectors, J. Virol. 78 (2004) 751–757.
[23] C.B. Buck, C.D. Thompson, Y.S. Pang, D.R. Lowy, J.T. Schiller, Maturation of papillomavirus capsids, J. Virol. 79 (2005) 2839–2846.
[24] D. Pyeon, P.F. Lambert, P. Ahlquist, Production of infectious human papillomavirus independently of viral replication and epithelial cell differentiation, Proc. Natl. Acad. Sci. USA 102 (2005) 9311–9316.
[25] H. Kimura, P. Cook, Kinetics of core histones in living human cells: Little exchange of H3 and H4 and some rapid exchange of H2B, J. Cell Biol. 153 (2001) 1341–1353.
[26] T. Buranda, G.M. Jones, J.P. Nolan, J. Keij, G.P. Lopez, L.A. Sklar, Ligand receptor dynamics at streptavidin-coated particle surfaces: A flow cytometric and spectrofluorimetric study, J. Phys. Chem. B 29 (1999) 3399–3410.
[27] S.E. Babbitt, A. Kiss, A.E. Deffenbaugh, Y.H. Chang, E. Bailly, H. Erdjument-Bromage, P. Tempst, T. Buranda, L.A. Sklar, J. Baumler, E. Gogol, D. Skowyra, ATP hydrolysis-dependent disassembly of the 26S proteasome is part of the catalytic cycle, Cell 20 (2005) 553–565.
[28] T. Buranda, J. M Huang, V.H. Perez-Luna, B. Schreyer, L.A. Sklar, G.P. Lopez, Biomolecular recognition on well-characterized beads packed in microfluidic channels, Anal. Chem. 1 (2002) 1149–1156.
[29] M.E. Piyasena, T. Buranda, Y. Wu, J.M. Huang, L.A. Sklar, G.P. Lopez, Near-simultaneous and real-time detection of multiple analytes in affinity microcolumns, Anal. Chem. 1 (2004) 6266–6273.
[30] P.C. Simons, M. Shi, T. Foutz, D.F. Cimino, J. Lewis, T. Buranda, W.K. Lim, R.R. Neubig, W.E. McIntire, J. Garrison, E. Prossnitz, L.A. Sklar, Ligand-receptor–G-protein molecular assemblies on beads for mechanistic studies and screening by flow cytometry, Mol. Pharmacol. 64 (2003) 1227–1238.
[31] P. Simons, C.M. Vines, T.A. Key, R.M. Potter, M. Shi, L.A. Sklar, E.R. Prossnitz (Eds.), Analysis of GTP-Binding Protein-Coupled Receptor Assemblies by Flow Cytometry, Oxford University Press, New York, 2005.
[32] A.J. Abbott, G.L. Nelsestuen, The collisional limit: An important consideration for membrane-associated enzymes and receptors, FASEB J. 2 (1988) 2858–2866.
[33] L.D. Shea, G.M. Omann, J.J. Linderman, Calculation of diffusion-limited kinetics for the reactions in collision coupling and receptor cross-linking, Biophys. J. 73 (1997) 2949–2959.
[34] A. Christopoulos, T. Kenakin, G protein-coupled receptor allosterism and complexing, Pharmacol. Rev. 54 (2002) 323–374.
[35] Q. Sun, J.M. Woodcock, C.J. Bagley, K. Jones, R. D'Andrea, A.F. Lopez, A monoclonal antibody (MoAb) to the human IL-3: GM-CSF and IL-5 receptor common beta-chain (β_c) neutralises the binding and function of all three ligands, Blood 88 (1996) 2170.
[36] S.P. Perfetto, P.K. Chattopadhyay, M. Roederer, Seventeen-colour flow cytometry: Unravelling the immune system, Nat. Rev. Immunol. 4 (2004) 648–655.
[37] T. Buranda, G. Jones, J. Nolan, J. Keij, G.P. Lopez, L.A. Sklar, Ligand receptor dynamics at streptavidin coated particle surfaces: A flow cytometric and spectrofluorimetric study, J. Phys. Chem. B 103 (1999) 3399–3410.
[38] L. B-Å. Johansson, A. Niemi, Electronic energy transfer in anistropic systems: I. Octadecylrhodamine B in vesicles, J. Phys. Chem. 91 (1987) 3020–3023.
[39] D.S. Lidke, P. Nagy, R. Heintzmann, D.J. Arndt-Jovin, J.N. Post, H.E. Grecco, E.A. Jares-Erijman, T.M. Jovin, Quantum dot ligands provide new insights into erbB/HER receptor-mediated signal transduction, Nat. Biotechnol. 22 (2004) 198–203.
[40] T.D. Culp, N.D. Christensen, Quantitative RT–PCR assay for HPV infection in cultured cells, J. Virol. Methods 111 (2003) 135–144.

[41] T.D. Culp, N.D. Christensen, Kinetics of in vitro adsorption and entry of papillomavirus virions, Virology 5 (2004) 152–161.
[42] J.C. Chung, N. Sciaky, D.J. Gross, Heterogeneity of epidermal growth factor binding kinetics on individual cells, Biophys. J. 73 (1997) 1089–1102.
[43] T. Domagala, N. Konstantopoulos, F. Smyth, R.N. Jorissen, L. Fabri, D. Geleick, I. Lax, J. Schlessinger, W. Sawyer, G.J. Howlett, A.W. Burgess, E.C. Nice, Stoichiometry, kinetic, and binding analysis of the interaction between epidermal growth factor (EGF) and the extracellular domain of the EGF receptor, Growth Factors 18 (2000) 11–29.
[44] K. Mayawala, D.G. Vlachos, J.S. Edwards, Heterogeneities in EGF receptor density at the cell surface can lead to concave up Scatchard plot of EGF binding, FEBS Lett. 6 (2005) 3043–3047.
[45] F. Ozcan, P. Klein, M.A. Lemmon, I. Lax, J. Schlessinger, On the nature of low- and high-affinity EGF receptors on living cells, Proc. Natl. Acad. Sci. USA 11 (2006) 5735–5740.
[46] S.M. Puddicombe, L. Wood, S.G. Chamberlin, D.E. Davies, The interaction of an epidermal growth factor transforming growth factor alpha tail chimera with the human epidermal growth factor receptor reveals unexpected complexities, J. Biol. Chem. 29 (1996) 30392–30397.
[47] M.R. Holbrook, L.L. Slakey, D.J. Gross, Thermodynamic mixing of molecular states of the epidermal growth factor receptor modulates macroscopic ligand binding affinity, Biochem. J. 15 (2000) 99–108.
[48] M.L. Blinov, J.R. Faeder, B. Goldstein, W.S. Hlavacek, A network model of early events in epidermal growth factor receptor signaling that accounts for combinatorial complexity, Biosystems 83 (2006) 2–3.
[49] H.T. Haigler, J.A. McKanna, S. Cohen, Direct visualization of the binding and internalization of a ferritin conjugate of epidermal growth factor in human carcinoma cells A-431, J. Cell Biol. 81 (1979) 382–395.
[50] D.S. Lidke, K.A. Lidke, B. Reiger, T.M. Jovin, D.J. Arndt-Jovin, Tracking erbB1 retrograde transport using quantum dot-labeled ligands, Biophys. J. 88 (2005) 8A.
[51] C. Lenzen, R.H. Cool, H. Prinz, J. Kuhlmann, A. Wittinghofer, Kinetic analysis by fluorescence of the interaction between Ras and the catalytic domain of the guanine nucleotide exchange factor Cdc25(Mm), Biochemistry 19 (1998) 7420–7430.
[52] J.M.M. Walboomers, M.V. Jacobs, M.M. Manos, F.X. Bosch, J.A. Kummer, K.V. Shah, P.J.F. Snijders, J. Peto, C.J.L.M. Meijer, N. Muñoz, Human papillomavirus is a necessary cause of invasive cervical cancer worldwide, J. Pathol. 189 (1999) 12–19.
[53] X.S. Chen, R.L. Garcea, I. Goldberg, G. Casini, S.C. Harrison, Structure of small virus-like particles assembled from the L1 protein of human papillomavirus 16, Mol. Cell. 5 (2000) 557–567.
[54] M. Favre, F. Breitburd, O. Croissant, G. Orth, Structural polypeptides of rabbit, bovine, and human papillomaviruses, J. Virol. 15 (1975) 1239–1247.
[55] D. Magde, G.E. Rojas, P.G. Seybold, Solvent dependence of the fluorescence lifetimes of xanthene dyes, Photochem. Photobiol. 70 (1999) 737–744.